Minimum pickup velocity

The transition between nano-scale and micro-scale

Anantharaman, Aditya; van Ommen, J. Ruud; Chew, Jia Wei

DOI
10.1002/aic.15527

Publication date
2017

Document Version
Final published version

Published in
AIChE Journal

Minimum Pickup Velocity: The Transition Between Nano-Scale and Micro-Scale

Aditya Anantharaman
School of Chemical and Biomedical Engineering, Nanyang Technological University, Singapore, Singapore

J. Ruud van Ommen
Dept. of Chemical Engineering, Delft University of Technology, Delft, The Netherlands

Jia Wei Chew
School of Chemical and Biomedical Engineering, Nanyang Technological University, Singapore, Singapore and Singapore Membrane Technology Center, Nanyang Environment and Water Research Institute, Nanyang Technological University, Singapore, Singapore

DOI 10.1002/aic.15527
Published online October 14, 2016 in Wiley Online Library (wileyonlinelibrary.com)

The transport of nano-scale particles has become increasingly important, but the knowledge base available is limited. This study aims to bridge the knowledge gap between the nano- and micro-scales for pneumatic conveying. A key parameter is the minimum pickup velocity (U_{pu}), which is the minimum fluid velocity required to initiate motion in a particle originally at rest. The U_{pu} values of nine alumina particles with particle diameters (d_p) ranging from 5 to 110,000 nm were determined using the weight loss method, then compared against the established pickup Zones (analogous to the Geldart Groups). Results indicated that: (1) U_{pu} varied non-monotonically with increasing d_p, thus revealing the missing link between the nano- and micro-scales; (2) the intermediate particle diameters surprisingly did not agree with any pickup Zone; (3) Zone III (analogous to Geldart Group C) is inadequate for all the nano-scale particles, so new boundaries and a new Zone are proposed. © 2016 American Institute of Chemical Engineers *AIChE J*, 63: 1512–1519, 2017

Keywords: minimum pickup velocity, gas-solid pneumatic conveying, nanoparticle agglomerate, nano-scale, micro-scale

Introduction

Industries, spanning oil and gas, and agro-processing, employ pneumatic conveying as an efficient, low-cost means of transporting particles. Unfortunately, particulate processes often operate on the basis of empirical correlations, although predictions are known to vary by orders-of-magnitude.[1,2] The reliance on empirical correlations rather than scientific principles is because of the lack of a more mechanistic understanding of such flow characteristics. The focus of the current study is on the minimum pickup velocity (U_{pu}) in gas-solid pneumatic conveying, specifically on the lesser known behaviors in the transition between nano-scale and micro-scale particles.

The minimum pickup velocity (U_{pu}) is the minimum fluid velocity required to initiate motion in a particle originally at rest,[3] below which the particles remain stationary and above which particles are entrained. This has important implications in pneumatic conveying as a guideline to balance sedimentation and clogging issues (when velocity is too low), and attrition and energy cost issues (when velocity is too high). The minimum pickup velocity (U_{pu}) in pneumatic conveying is analogous to the minimum fluidization velocity (U_{mf}) in fluidization systems,[4–6] in that both dictate the minimum fluid velocity required for operating such fluid-solid operations.

Most of the efforts on minimum pickup velocity (U_{pu}) focus on larger particles with particle diameters (d_p) on the order of micrometer (μm) and some on the lower-end of the millimeter (mm) scale (the largest used for comparison in this study was 3.5 mm). For brevity, all particles with diameters (d_p) on the order of micro- and millimeter are referred to as "micro-scale" particles throughout this study. One of the earlier efforts[7] proposed a visual technique to determine U_{pu} and investigated particles in the particle diameter (d_p) range of 7–800 μm. A non-monotonic (specifically, decreased then increased) relationship between U_{pu} and d_p was revealed. This was attributed to the dominance of inter-particle cohesive forces at lower d_p values and inertial forces at higher d_p values. A semi-empirical model involving the Reynolds number (Re) and the Archimedes number (Ar) was also developed. An empirical correlation for determining U_{pu} as a function of particle diameter (d_p), particle Reynolds number (Re_p), particle density (ρ_p), and gas density (ρ) using dimensional analysis was also developed.[8] Subsequently, the non-monotonic relationship was further affirmed by Hayden et al.,[9] who investigated particles from Geldart Groups A and C.[10]

A three-zone model to classify the different particulate behavior, analogous to that established by Geldart for

Correspondence concerning this article should be addressed to J. W. Chew at JChew@ntu.edu.sg.

bubbling fluidized beds,[10] was proposed for pneumatic conveying.[11] The classification is based on a plot of the modified particle Reynolds number (Re_p*; modified to account for differences in channel diameter) and the Archimedes number (Ar).[11] Specifically, to enable a fair comparison across the various studies, Kalman et al.[11] proposed a correlation to normalize the effect of different diameters of the pneumatic conveying channels used with respect to that of a channel diameter of 50 mm:

$$\frac{U_{pu}}{U_{pu,50}} = 1.4 - 0.8 \cdot e^{-\frac{D/D_{50}}{1.5}} \quad (1)$$

where U_{pu} is the minimum pickup velocity, $U_{pu,50}$ is the minimum pickup velocity normalized for a channel inner diameter of 50 mm, D is the inner diameter of the pneumatic conveying channel, and D_{50} is the reference channel diameter of 50 mm. This normalization improved on that proposed by Cabrejos and Klinzing[8] earlier, whereby $U_{pu} \propto D^{0.25}$. The correlations for the three zones are expressed as follows[11]:

$$\text{Zone I}: Re_p^* = 5Ar^{\frac{1}{7}} \text{ for } Ar \geq 16.5 \quad (2)$$

$$\text{Zone II}: Re_p^* = 16.7 \text{ for } 0.45 < Ar < 16.5 \quad (3)$$

$$\text{Zone III}: Re_p^* = 21.8Ar^{\frac{1}{3}} \text{ for } Ar \leq 0.45 \quad (4)$$

where Ar stands for the Archimedes number defined as:

$$Ar = \frac{g\rho(\rho_p - \rho)d_p^3}{\mu^2} \quad (5)$$

and Re_p* represents the particle Reynolds number that is modified to account for different channel diameters[11]:

$$Re_p^* = \frac{\rho d_p U_{pu}}{\mu\left(1.4 - 0.8e^{-\frac{D/D_{50}}{1.5}}\right)} \quad (6)$$

where g is the gravitational acceleration, ρ_p is the particle density, ρ is the density of ambient air, and μ is the ambient air viscosity. Zone I has been reported to correspond approximately to Geldart Groups B and D, while Zones II and III to Geldart Groups A and C, respectively.[11–14] This three-zone model was later incorporated into the "generalized master curve" by Rabinovich and Kalman.[15]

However, such a classification was developed based on micro-scale particles only, hence its applicability for the increasingly popular conveying of nano-scale particles (e.g., nanoparticle synthesis,[16] inhalers for drug delivery,[17,18] and air pollution[19,20]) may be limited. Because of the significant inter-particle cohesive forces, such as London-van der Waals, electrostatic, and moisture-induced surface tension forces, nano-scale particles exist as agglomerates rather than individual particles.[21,22] Consequently, the minimum fluidization velocity (U_{mf}) of nano-scale particles has been reported to be orders-of-magnitude greater than that of micro-scale particles.[23–27] Furthermore, two types of fluidization behaviors unique to nano-scale particles are known, namely, agglomerate particulate fluidization (APF) and agglomerate bubbling fluidization (ABF).[21,26] Regarding pneumatic conveying of nano-scale particles, our recent study[12] found that the Zones[11] are not strictly applicable for nanoparticles. Key findings on the minimum pickup velocity (U_{pu}) of polar and apolar nanoparticles of three different materials in the particle diameter (d_p) range of 13–21 nm include[12]: (1) the U_{pu} values were at least an order-of-magnitude lower than that expected from the three-zone model due to agglomeration, and (2) although nanoparticles belong in Zone III, while the complex agglomerates[28] of the nanoparticles complied with the Zone I correlation, calculations based on the individual nanoparticle properties indicated that these complied with the extrapolated Zone I correlation. Clearly, nano-scale particles exhibit behavior different from their micro-scale counterparts.

Armed with the knowledge on the minimum pickup velocity (U_{pu}) trends of micro-scale and that the behavior of nano-scale particles cannot be predicted by the classification developed based on micro-scale particles, this study aims at bridging the gap in terms of (1) understanding the underlying discrepancy in behavior between the nano-scale particles and the lower range of micro-scale particles (i.e., Zone III or Geldart Group C), and (2) determining when the transition between nano-scale and micro-scale occurs. The behavior of alumina (Al_2O_3) particles with particle diameters (d_p) between 21 nm[12] (i.e., nano-scale) and 530 nm[9] (i.e., lowest bound of micro-scale) in terms of minimum pickup velocity (U_{pu}) is currently not known, so this study investigates particles in the particle diameter (d_p) range of 5 nm and 110,000 nm, hence traversing both scales. The scope of the study is limited to understanding the behavioral differences between the nano- and micro-scale particles in practical pneumatic conveying applications via the U_{pu} values; the detailed unraveling of the underlying physics particularly of the various inter-particle cohesive effects (e.g., van der Waals, electrostatics) of the nano-scale particles leading to the differences is unfortunately beyond the scope of the current study.

Materials and Methods

Experimental setup

The experimental setup schematically depicted in Figure 1 was identical to that used in previous studies.[12,13] The pneumatic conveying setup was a hollow acrylic tube, and consisted of three sections, namely, A, B, and C, which could be connected by means of screws and flanges. The inner diameter was 16 mm internal diameter and the wall thickness was 2 mm. Section A, the inlet section, was connected to the central air supply with a maximum flow rate of 0.0015 m^3/s. Section B, the sample section, consisted of two semi-cylindrical halves, the bottom half of which was packed to the brim with plasticine up to a length of 27.5 cm from the inlet side, while the remaining 2.5 cm served as a chamber to hold the sample under investigation. More specifically, the surface of the particle sample was flat and of the same level as the plasticine to ensure that the cross-sectional area of airflow remained constant throughout Section B. This enabled the pickup velocity (U_{pu}) to be measured to a greater degree of accuracy compared to the method involving a varying cross-sectional area.[7–9] The lengths of the inlet (Section A) and exit (Section C) sections were made sufficiently long to ensure a fully developed airflow before the particle sample and minimize exit effects, respectively. The outlet air stream was passed through water first and then through a High Efficiency Particulate Arrestance (HEPA) filter to avoid the release of the nanoparticles into the environment.[29] Experiments were carried out at room temperature (approximately 25°C). The relative humidity values in the laboratory and in the inlet gas stream were monitored to be $56\% \pm 2\%$ and $27\% \pm 2\%$, respectively, throughout the experiments. Electrostatic effects, acknowledged to be

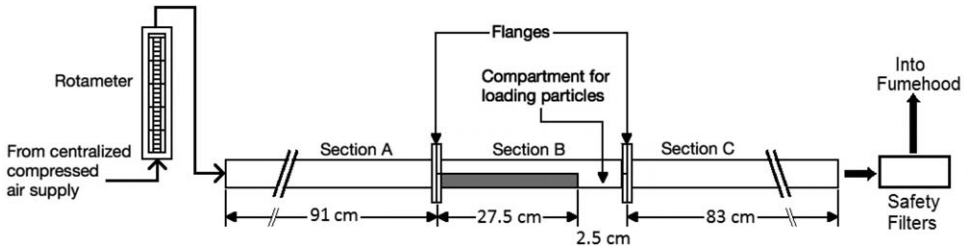

Figure 1. Experimental setup.

negligible compared to the Van der Waals forces,[29,30] were not considered in this study.

Materials

Alumina (Al_2O_3) particles in the particle diameter (d_p) range of 5 to 300 nm were obtained from US-Nano, and with the particle diameters (d_p) of 20,000 and 110,000 nm were obtained from Sasol. Alumina (Al_2O_3) particles have a particle density (ρ_p) of 3600 kg/m^3. The polymorph types (i.e., gamma or alpha) and particle diameters (d_p) of the nine samples are listed in Table 1. The particles were used as is. It should be noted that the particle diameters (d_p) were provided by the vendors, who did not provide the particle-size distributions (PSDs), although it has been reported that changes in PSDs affect the pickup velocity (U_{pu}) for micro-scale particles.[13] Efforts to obtain the PSDs for the nanoparticles via a nanosizer (BIC 90Plus) were futile since larger mean particle diameters (d_p) than those provided by the vendor were obtained presumably due to insufficient dispersion of the nanoparticle agglomerates.

Procedure to measure U_{pu}

The "weight loss" method, first implemented by Kalman et al.[11] for micro-scale particles then subsequently applied for nano-scale particles,[12] was employed in this study. Specifically, the method devised by Kalman et al.[11] is distinctly different in that the constant cross-sectional area is expected to confer less errors than earlier methods with varying cross-sectional areas as the particle heap erodes.[7–9] The minimum pickup velocity (U_{pu}) is defined as the air velocity at which mass loss due to entrainment becomes non-zero.[11] Briefly, the steps taken were as follows: (1) the particle sample was loaded into the sample chamber in the bottom semi-cylindrical half of Section B and weighed, (2) all sections of the pneumatic conveying setup were securely connected, (3) airflow at the desired rate was implemented for a duration of 120 s, and (4) the bottom semi-cylindrical half of Section B was dismantled and weighed. The same protocol was repeated for a range of airflow rates. At least three repeats were performed for each data point to ensure reproducibility. Figure 2 shows a typical mass loss curve, which is a plot of mass loss from Section B vs. air velocity, obtained for the particles with a gamma polymorph type and particle diameter (d_p) of 20 nm. The minimum pickup velocity (U_{pu}) was determined as the air velocity at which the extrapolated mass loss curve intersects with the x axis, since U_{pu} is by definition the air velocity at which entrainment (i.e., mass loss) just becomes non-zero.

Table 1. Relevant Properties of the Alumina (Al_2O_3) Particles Investigated

d_p (nm)	Polymorph type
5	Gamma
20	Gamma
80	Gamma
80	Alpha
135	Alpha
200	Alpha
300	Alpha
20,000	Gamma
110,000	Gamma

Results and Discussion

Figure 3 displays minimum pickup velocity (U_{pu}) and normalized minimum pickup velocity ($U_{pu,50}$; Eq. 1) vs. particle diameter (d_p), specifically the individual particle diameters (d_p) listed in Table 1, on a semi-logarithmic plot of all the particle samples investigated in this study. Data from four previous studies are also portrayed: three of them were included because alumina particles were similarly studied,[7,9,12] while one was on zirconium particles ($\rho_p = 5964$ kg/m^3) because it represented the uppermost limit of Ar investigated to date.[11] Four short notes on the data obtained in this study depicted in Figure 3 include (1) the trends for U_{pu} (Figure 3a) and $U_{pu,50}$ (Figure 3b) are very similar, which implies that the normalization with respect to pipe diameter (Eq. 1) does not significantly affect the overall trends; (2) the U_{pu} magnitudes for the particles with $d_p = 5$–135 nm were an order-of-magnitude lower than that for micro-scale particles investigated in previous efforts,[7,9,11] which is consistent with the data for the nano-

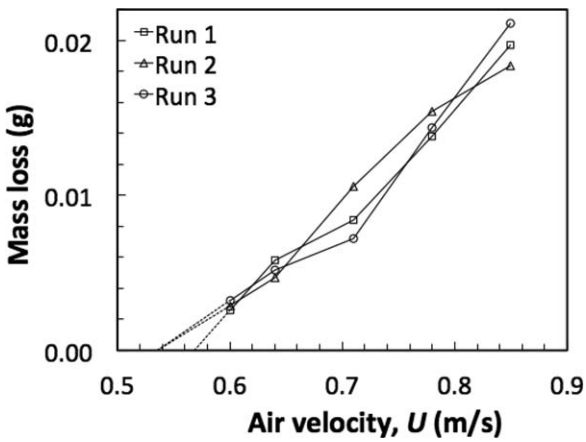

Figure 2. Mass loss curves of alumina particles with a gamma polymorph type and particle diameter (d_p) of 20 nm for three repeats.

In this case, the minimum pickup velocity (U_{pu}) values were determined as 0.536 m/s, 0.536 m/s, and 0.568 m/s, hence the characteristic U_{pu} was averaged to be 0.547 ± 0.032 m/s.

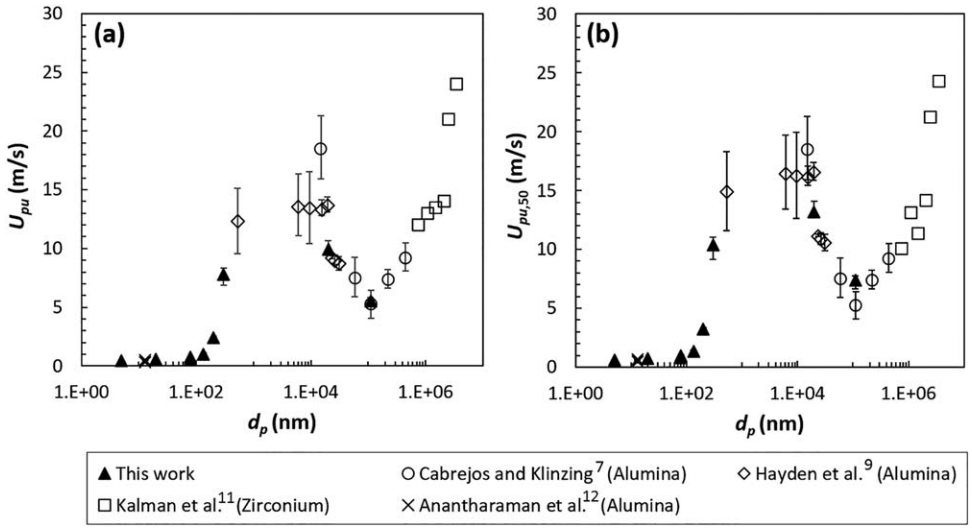

Figure 3. Comparison of experimental results from this study (the d_p values on the x axis are of the individual particles listed in Table 1) with those from previous studies[7,9,11,12]: (a) minimum pickup velocity (U_{pu}), and (b) normalized minimum pickup velocity ($U_{pu,50}$; Eq. 1).

scale particles with $d_p = 13$–21 nm obtained by our previous study[12]; (3) the U_{pu} characterized for the alumina particles with $d_p = 20{,}000$ and 110,000 nm agreed qualitatively with the data obtained by previous studies[7,9]; and (4) the difference between the U_{pu} values of the alpha and gamma variants of the alumina particles with $d_p = 80$ nm (Table 1) was not significant, hence the effect of polymorph type can be considered as negligible.

The significant highlight in Figure 3 is that the U_{pu} values exhibited a non-monotonic trend with respect to d_p. Specifically, U_{pu} increased slowly between $d_p = 5$–80 nm then quickly till $d_p = 530$ nm, followed by a plateau between $d_p = 530$–$15{,}000$ nm, after which a decrease between $d_p =$ 15,000–110,000 nm before increasing beyond $d_p =$ 110,000 nm. For the nano-scale particles, although they belong to Zone III (or Geldart Group C), it was found earlier that they surprisingly behaved more like Zone I (or Geldart Group B) particles due to agglomeration effects.[12] Conversely, for the micro-scale particles ($d_p \geq 530$ nm), a non-monotonic trend has been reported in that U_{pu} plateaued then decreased with d_p in Zones III and II (or Geldart Groups C and A, respectively) due to decreasing inter-particle cohesion effects, then increased with d_p in Zone I (or Geldart Group B) due to increasing inertial effects.[7,9] Notably, Figure 3 serves to reveal the missing link on the pneumatic conveying behavior of particles between $d_p = 5$ nm (i.e., nano-scale) and $d_p = 530$ nm[9] (i.e., micro-scale) in terms of U_{pu} trends.

Figure 4 illustrates the plot of Re_p* (Eq. 6) vs. Ar (Eq. 5), whereby the d_p values substituted were those of the individual particles listed in Table 1. The solid lines represent the three correlations for each of the zones (Eqs. 2–4), while the dotted line represents the extrapolated Zone I correlation (Eq. 2). Each discrete data point represents each of the nine particle samples (Table 1). Three observations are notable from Figure 4. First, the particles with $d_p = 20{,}000$ and 110,000 nm agreed exactly with the Zone II and Zone I correlations, respectively, which is expected. For such micro-scale particles, the smaller ones in Zone I experience some inter-particle cohesion effects, while the larger ones tend to be entrained as individual particles.[7,9,11] Second, although nano-scale particles belong to Zone III, the particles with particle diameter (d_p) up to 135 nm agreed well with the extrapolated Zone I correlation. This is similar to the observations in our previous study,[12] which attributed it to agglomeration effects[28] that leads to micro-scale agglomerates rather than nano-scale particles being entrained. Third and perhaps most notably, the particles with $d_p = 200$ and 300 nm agreed with none of the three zones. More specifically, these two particle samples lie in between the extrapolated Zone I and Zone III correlations, which indicated an intermediate mechanism between the pneumatic conveying of micro-scale agglomerates (Zone I) and smaller agglomerates (Zone III).

To estimate the characteristic diameters (d^{**}) and densities (ρ^{**}) of the complex nanoparticle agglomerates, the force balance model presented in our previous study[12] was employed. This model was adopted from de Martin and van Ommen,[28] wherein the diameters of complex nanoparticle agglomerates

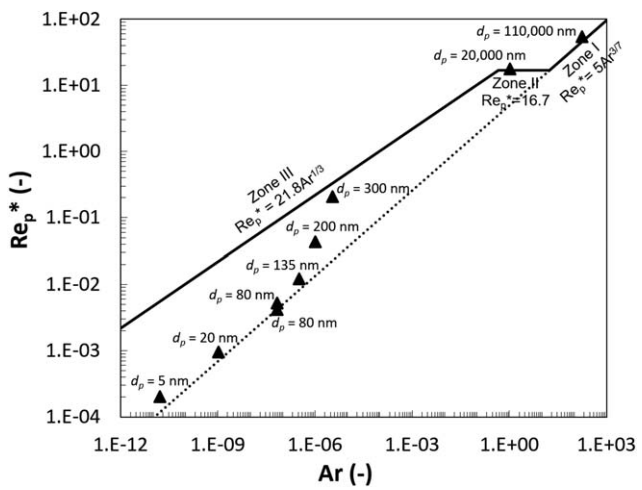

Figure 4. Re_p* vs. Ar for the particle samples investigated.

The solid lines represent the three correlations for each of the zones and the dotted line represents the extrapolated Zone I correlation. Each discrete data point represents each of the nine particle samples. Re_p* (Eq. 6) and Ar (Eq. 5) were calculated using the individual particle diameter (d_p) listed in Table 1.

Table 2. Properties of Primary[34,38] and Complex[28] Agglomerates of Nano-Scale Particles

d_p (nm)	Primary agglomerate diameter, d^* (nm)	Primary agglomerate density, ρ^* (kg/m^3)	Complex agglomerate diameter, d^{**} (nm)	Complex agglomerate density, ρ^{**} (kg/m^3)
5	35,000	104.29	669,500	5.45
20	35,000	181.59	374,900	16.95
80	35,000	316.16	196,600	56.28
80	35,000	316.16	196,600	56.28
135	35,000	389.77	161,000	84.73
200	35,000	456.13	141,400	112.90
300	35,000	536.44	125,600	149.49

Note that the particles with $d_p = 20{,}000$ and 110,000 nm are excluded as unphysical d^{**} values were obtained.

formed during dry nano-scale particle fluidization was calculated based on inter-particle cohesive forces. Table 2 provides the properties (namely, particle diameter and particle density) of the primary and complex nanoparticle agglomerates. Specifically, nanoparticle agglomerates have been found to possess a hierarchical structure,[31,32] as in that primary nanoparticle agglomerates[33–36] of diameter d^* are first created which further agglomerate to form complex agglomerates[28,33] of diameter d^{**}. It should be noted that the particles with $d_p = 20{,}000$ and 110,000 nm were omitted from Table 2, because the agglomerate diameters so obtained were smaller than the individual particle diameter, which is not physical. Three noteworthy observations are obtained from Table 2. First, the diameters of the complex agglomerates (d^{**}) were of the order 10^5 nm, which is three to five orders-of-magnitude greater than the individual particle diameter (Table 1), while the complex agglomerate density (ρ^{**}) were 10^1 to 10^2 kg/m^3, which is one to three orders-of-magnitude smaller than the individual particle density. This is consistent with the results of our previous study.[12] Second, as the individual particle diameter (d_p) increased, the complex agglomerate diameter (d^{**}) decreased while the complex agglomerate density (ρ^{**}) increased, which indicates the decreased inter-particle cohesion effect and the decreased porosity of the resulting agglomerates. Third, the ρ^{**} value corresponding to the particle diameter (d_p) of 5 nm particles appears to be low at 5.5 kg/m^3, which translates to an unexpectedly high particle porosity of 0.999. This is perhaps not as surprising considering: (1) the ρ^{**} and porosity values of particles with $d_p = 12$–13 nm have been reported to be 13 kg/m^3 [31,36,37] and 0.997,[37] respectively; and (2) an error of up to $\pm 30\%$ in the prediction of d^{**} by the model has been acknowledged,[28] and since the model was developed only for particle diameter, the values for density and porosity may be subject to even greater errors.

Regarding the nature of the entities (i.e., particles or agglomerates) being pneumatically conveyed, the gradient of the mass loss curve (Figure 2) provides a good indication. Accordingly, the gradients of all the mass loss curves were computed by linear regression analyses of the five or six points constituting each curve. The linear regression coefficient (R^2) values were all greater than 0.94, which implied reasonable goodness of fit and hence that the mass loss curves were approximately straight lines for the five or six data points corresponding to air velocities (U) just above the minimum pick-up velocity (U_{pu}). Figure 5 shows the average slopes of the linearly regressed mass loss curves vs. particle diameter (d_p), specifically the individual particle diameters (d_p) listed in Table 1, on a semi-logarithmic plot. Each error bar indicates the span of values for the three repeats carried out. The average slope is approximately invariant with particle diameter (d_p) for $d_p \leq 135$ nm, then clearly decreases before increasing with d_p. The zones depicted in Figure 4 can also be seen in Figure 5, which also serves to provide a mechanistic understanding of the nature of the entities being entrained. Regarding Zone I, particles with $d_p \leq 135$ nm and $d_p = 110{,}000$ nm were classified into this zone (Figure 4), which is such that the entrained particles or agglomerates are on the micro-scale (Table 2). In Figure 5, Zone I is represented by larger slope magnitudes, which indicate the entrainment of larger entities beyond the minimum pickup velocity (U_{pu}). With respect to Zone II, particles with $d_p = 20{,}000$ nm were categorized into this zone (Figure 4), which is such that the entrained particles are not individual particles due to inter-particle cohesion, but the cohesion effects are not adequately significant for the agglomerates to be the size of the entities entrained in Zone I. In Figure 5, Zone II is represented by the smallest slope magnitude. Finally, the particles with $d_p = 200$ nm and 300 nm agreed with neither of the three zones in Figure 4 and are represented by slope magnitudes in between those for Zones I and II in Figure 5.

Figure 6 shows the Re_p^* against Ar plot for the primary and complex agglomerates of the particles with particle diameters (d_p) of 5–300 nm (Table 2). In contrast to Figure 4, the particle diameter (d_p) values used in the calculation of Re_p^* (Eq. 6) and Ar (Eq. 5) are those of the primary and complex agglomerates listed in Table 2. Figure 4 has shown that particles in the particle diameter (d_p) range of 5–135 nm agreed well with

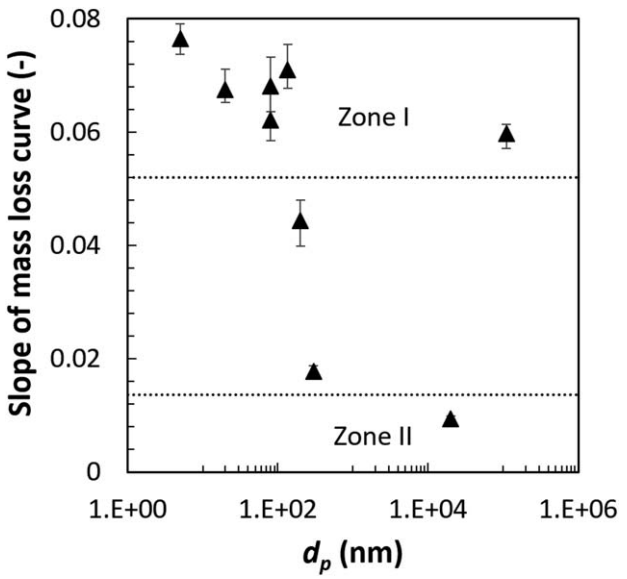

Figure 5. Slope of the linearly regressed mass loss curves vs. particle diameter (d_p), specifically the individual particle diameters (d_p) listed in Table 1.

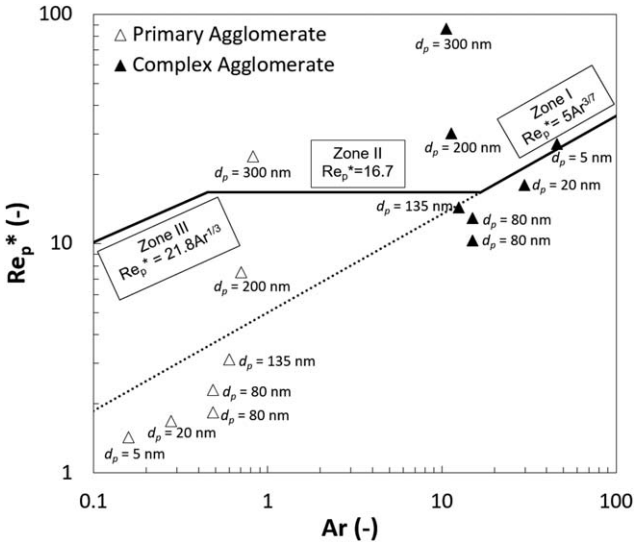

Figure 6. Re_p^* vs. Ar plot of the primary agglomerates and complex agglomerates for the particles with d_p = 5–300 nm (Table 2).

The solid lines represent correlations for the three pick-up zones and the dotted line represents the extrapolated Zone I correlation. Re_p^* (Eq. 6) and Ar (Eq. 5) were calculated using the primary (d^*) or complex (d^{**}) nanoparticle diameters listed in Table 2.

the extrapolated Zone I correlation, while the two particle samples with $d_p = 200$ and 300 nm did not agree with any of the Zone. Here, Figure 6 indicates that, for particles with $d_p = 5$–135 nm, the primary agglomerates agreed somewhat with the extrapolated Zone I correlation, while the complex agglomerates agreed with the Zone I correlation. This is consistent with a previous study for particle diameters (d_p) in the range of 13–21 nm.[12] In addition, both the primary and complex agglomerates of the particle samples with $d_p = 200$ and 300 nm persist in not agreeing well with any Zone.

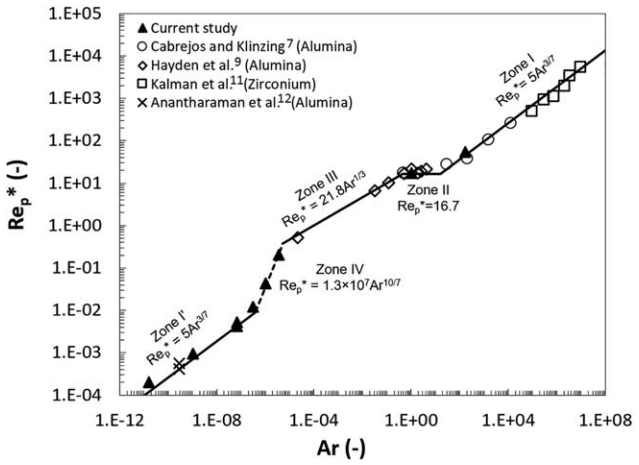

Figure 7. Re_p^* vs. Ar for particles (5–3,500,000 nm) representing the entire range of Re_p^* and Ar values investigated to date.[7,9,11,12]

The solid lines represent correlations for Zones I, II, III, and I' and the dotted line represents the newly proposed Zone IV. Each discrete datapoint represents each particle species investigated. Re_p^* (Eq. 6) and Ar (Eq. 5) were calculated using the individual particle diameter (d_p) listed in Table 1.

To further assess the categorization of particles into Zones[11] for the intermediate particle diameters, Figure 7 summarizes the minimum pick-up velocity (U_{pu}) data to date, per those depicted in Figure 4, in a plot of Re_p^* against Ar. Similar to Figure 4, the d_p values substituted were those of the primary particles listed in Table 1. The data is representative of the entire range of Re_p^* and Ar values investigated to date, which spans particle diameters (d_p) of 5 nm to 3.5 mm at a particle density (ρ_p) of 3600 kg/m^3 (alumina) or 5964 kg/m^3 (zirconium). As mentioned earlier, the study on zirconium particles was included because it represented the highest values of Ar investigated to date. Figure 7 indicates that, other than the well-acknowledged Zones I, II, and III, further Zones are plausible for the lower Re_p^* and Ar magnitudes, which thereby imposes a lower bound for Zone III. This is because of the varying inter-particle cohesion and hence agglomeration behaviors of the nano-scale particles due to the well-acknowledged effects of London-van der Waals, electrostatic, and moisture-induced surface tension forces.[21,22] It should be noted that the pickup of agglomerates rather than individual particles has been acknowledged for Zone III,[11] but the nano-scale particles investigated in this study appear to suggest that the extents of agglomeration may be different. On the one hand, for the smallest particle diameters (d_p) investigated in this study of 5–135 nm, the agglomeration was so extensive such that the resulting agglomerates became large enough to behave like the micro-scale particles in Zone I. This proposed extrapolation of Zone I is labeled as Zone I' in Figure 7. It should be noted that Zone I has been reported to be applicable for smaller Ar ranges for the pickup of particles in liquid-solid systems,[39] but the underlying reasons are distinctly different. Whereas the extrapolation here was due to extensive cohesive effects leading to complex agglomerates, that in Rabinovich and Kalman[39] was attributed to the negligible van der Waals forces in liquid-solid systems for the Ar range in which cohesive forces are significant in gas-solid systems.[39] On the other hand, for the intermediate particle diameters (d_p) investigated of 200–300 nm, a new Zone seems to exist in which the particles exhibited inter-particle cohesion effects intermediate between those of the original Zones III and I'. This new Zone is termed Zone IV, since it deviates from the available correlations defining the Zones. The intermediate behavior is presumably due to the coupled effects of increased van der Waals but decreased electrostatics interactions compared to that of Zone III, the same effects of which led to a weaker hierarchical structure of the agglomerates than that of Zone I'. Further studies on understanding the balance between the opposing effects of van der Waals and electrostatics interactions for nano-scale particles are necessary.

The correlation and bounds for Zones I and II remain unchanged. Under Zone I', a new range of particles at the lowest end of Re_p^* and Ar is suggested:

$$\text{Zone I}' : \mathrm{Re}_p^* = 5\mathrm{Ar}^{\frac{3}{7}} \text{ for } \mathrm{Ar} \leq 4\times10^{-7} \tag{7}$$

For Zone III, a new lower bound can be drawn, which can be expressed as:

$$\text{Zone III} : \mathrm{Re}_p^* = 21.8\mathrm{Ar}^{\frac{1}{3}} \text{ for } 5\times10^{-6} \leq \mathrm{Ar} \leq 0.45 \tag{8}$$

As for the conceivable Zone IV in between Zones I' and III, the following correlation can be postulated:

$$\text{Zone IV} : \mathrm{Re}_p^* = 1.3\times10^7\mathrm{Ar}^{\frac{10}{7}} \text{ for } 4\times10^{-7} < \mathrm{Ar} < 5\times10^{-6} \tag{9}$$

As only two of the particle samples investigated here fall into Zone IV, more data points would be beneficial to improving the correlation.

Conclusion

Experiments were conducted to determine the minimum pickup velocity (U_{pu}) of nine samples of alumina (Al_2O_3) particles with particle diameters (d_p) traversing the nano-scale and micro-scale (specifically in the range of 5–110,000 nm) by the weight loss method. This serves to reveal the missing link on the pneumatic conveying behavior of particles between $d_p = 21$ nm[12] and $d_p = 530$ nm[9] in terms of U_{pu} trends. The U_{pu} values obtained were then used to categorize the particles using the well-acknowledged three-zone classification.[11]

The three key highlights are as follows. First, the minimum pickup velocity (U_{pu}) determined in this study exhibited a non-monotonic trend with respect to particle diameter (d_p) in the d_p range of 5 nm to 3.5 mm. Specifically, U_{pu} increased up to $d_p = 530$ nm, plateaued till $d_p = 15{,}000$ nm, then decreased till $d_p = 110{,}000$ nm before increasing again. Notably, the missing link revealed on the pneumatic conveying behavior of particles is that between $d_p = 5$ nm (i.e., nano-scale) and $d_p = 530$ nm[9] (i.e., micro-scale) in terms of U_{pu} trends. Second, while the particles in the particle diameter (d_p) range of 5–135 nm agreed with the extrapolated Zone I correlation due to agglomeration effects, the two largest particle diameters (d_p) of 20,000 and 110,000 nm were expectedly classified, respectively, into Zones II and I; however, the intermediate particle diameters (d_p) of 200 and 300 nm could not be classified into any of the three zones. Third, Zone III per se is inadequate in accounting for all the smaller cohesive particles, because of varying extents of inter-particle cohesion and hence agglomeration. For the particles investigated in this study which were expected to be categorized as Zone III, while the smallest ones (in this case, $d_p = 5$–135 nm) agglomerated so extensively such that the agglomerates became large enough to behave like the micro-scale particles in Zone I, the intermediate ones (in this case, $d_p = 200$–300 nm) did not agree with the Zone III correlation. Hence, within the original Zone III, a lower bound for Ar is suggested such that a new Zone IV can be labeled, along with Zone I' (i.e., the proposed extrapolation of Zone I) for the lowest ranges of Ar.

The findings of this study thus indicate that the minimum pickup velocity (U_{pu}) of nano-scale particles deviates from that expected from understanding based on micro-scale particles. This underscores the need for bridging the gap between the two scales.

Acknowledgment

The authors thank the financial support from the National Research Foundation (NRF), Prime Minister's Office, Singapore under its Campus for Research Excellence and Technological Enterprise (CREATE) program.

Literature Cited

1. Chew JW, Cahyadi A, Hrenya CM, Cocco R. Review of entrainment correlations in gas-solid fluidization. *Chem Eng J*. 2015;260:152–171.
2. Cahyadi A, Chew JW, Hrenya CM, Cocco RA. Comparative study of transport disengaging height (TDH) correlations in gas–solid fluidization. *Powder Technol*. 2015;275:220–238.
3. Halow JS. Incipient rolling, sliding and suspension of particles in horizontal and inclined turbulent flow. *Chem Eng Sci*. 1973;28:1–12.
4. Wen CY, Yu YH. Mechanics of fluidization. *Chem Eng Prog Symp Ser*. 1966;62:100–111.
5. Kunii D, Levenspiel O. Fluidization and mapping of regimes. In: Kunii D, Levenspiel O, editors. *Fluidization engineering*, 2nd ed. Boston: Butterworth-Heinemann, 1991:61–94.
6. Fan L-S, Zhu C. Dense-phase fluidized beds. In: Fan L-S, Zhu C, editors. *Principles of gas-solid flows*. Cambridge: Cambridge University Press, 1998:371–420.
7. Cabrejos FJ, Klinzing GE. Incipient motion of solid particles in horizontal pneumatic conveying. *Powder Technol*. 1992;72:51–61.
8. Cabrejos FJ, Klinzing GE. Pickup and saltation mechanisms of solid particles in horizontal pneumatic transport. *Powder Technol*. 1994; 79:173–186.
9. Hayden KS, Park K, Curtis JS. Effect of particle characteristics on particle pickup velocity. *Powder Technol*. 2003;131(1):7–14.
10. Geldart D. Types of gas fluidization. *Powder Technol*. 1973;7:285–292.
11. Kalman H, Satran A, Meir D, Rabinovich E. Pickup (critical) velocity of particles. *Powder Technol*. 2005;160(2):103–113.
12. Anantharaman A, van Ommen JR, Chew JW. Minimum pickup velocity (U_{pu}) of nanoparticles in gas–solid pneumatic conveying. *J Nanopart Res*. 2015;17(12):470.
13. Anantharaman A, Wu X, Hadinoto K, Chew JW. Impact of continuous particle size distribution width and particle sphericity on minimum pickup velocity in gas–solid pneumatic conveying. *Chem Eng Sci*. 2015;130:92–100.
14. Goy SP, Chew JW, Hadinoto K. Effects of binary particle size distribution on minimum pick-up velocity in pneumatic conveying. *Powder Technol*. 2011;208(1):166–174.
15. Rabinovich E, Kalman H. Generalized master curve for threshold superficial velocities in particle–fluid systems. *Powder Technol*. 2008;183(2):304–313.
16. Shabeer A, Chandrashekhara K, Schuman T. Synthesis and characterization of soy-based nanocomposites. *J Compos Mater*. 2007; 41(15):1825–1849.
17. Gandhimathi C, Venugopal JR, Sundarrajan S, Sridhar R, Tay SS, Ramakrishna S, Kumar SD. Breathable medicine: pulmonary mode of drug delivery. *J Nanosci Nanotechnol*. 2015;15(4):2591–2604.
18. Sham JOH, Zhang Y, Finlay WH, Roa WH, Löbenberg R. Formulation and characterization of spray-dried powders containing nanoparticles for aerosol delivery to the lung. *Int J Pharm*. 2004;269(2): 457–467.
19. Niu J, Rasmussen PE, Hassan NM, Vincent R. Concentration distribution and bioaccessibility of trace elements in nano and fine urban airborne particulate matter: influence of particle size. *Water Air Soil Pollut*. 2010;213(1–4):211–225.
20. Stahlmecke B, Wagener S, Asbach C, Kaminski H, Fissan H, Kuhlbusch TAJ. Investigation of airborne nanopowder agglomerate stability in an orifice under various differential pressure conditions. *J Nanopart Res*. 2009;11(7):1625–1635.
21. Zhu C, Yu Q, Dave RN, Pfeffer R. Gas fluidization characteristics of nanoparticle agglomerates. *AIChE J*. 2005;51(2):426–439.
22. Hakim LF, Portman JL, Casper MD, Weimer AW. Aggregation behavior of nanoparticles in fluidized beds. *Powder Technol*. 2005; 160(3):149–160.
23. Jung JW, Gidaspow D. Fluidization of nano-size particles. *J Nanopart Res*. 2002;4(6):483–497.
24. Morooka S, Kusakabe K, Kobata A, Kato Y. Fluidization state of ultrafine powders. *J Chem Eng Jpn*. 1988;21(1):41–46.
25. Pacek AW, Nienow AW. Fluidization of fine and very dense hardmetal powders. *Powder Technol*. 1990;60(2):145–158.
26. Wang Y, Gu GS, Wei F, Wu J. Fluidization and agglomerate structure of SiO_2 nanoparticles. *Powder Technol*. 2002;124(1–2):152–159.
27. Wang ZL, Kwauk M, Li HZ. Fluidization of fine particles. *Chem Eng Sci*. 1998;53(3):377–395.
28. de Martín L, van Ommen JR. A model to estimate the size of nanoparticle agglomerates in gas−solid fluidized beds. *J Nanopart Res*. 2013;15(11):
29. Tahmasebpoor M, de Martin L, Talebi M, Mostoufi N, van Ommen JR. The role of the hydrogen bond in dense nanoparticle-gas suspensions. *Phys Chem Chem Phys*. 2013;15(16):5788–5793.
30. Valverde JM, Quintanilla MAS, Espin MJ, Castellanos A. Nanofluidization electrostatics. *Phys Rev E*. 2008;77:(3):031301
31. de Martín L, Fabre A, van Ommen JR. The fractal scaling of fluidized nanoparticle agglomerates. *Chem Eng Sci*. 2014;112:79–86.
32. Yao W, Guangsheng G, Fei W, Jun W. Fluidization and agglomerate structure of SiO_2 nanoparticles. *Powder Technol*. 2002;124:152–159.

33. Castellanos A, Valverde JM, Quintanilla MAS. Aggregation and sedimentation in gas-fluidized beds of cohesive powders. *Phys Rev E*. 2001;64:(4):041304
34. Nam CH, Pfeffer R, Dave RN, Sundaresan S. Aerated vibrofluidization of silica nanoparticles. *AIChE J*. 2004;50(8):1776–1785.
35. Quintanilla MAS, Valverde JM, Espin MJ, Castellanos A. Electrofluidization of silica nanoparticle agglomerates. *Ind Eng Chem Res*. 2012;51(1):531–538.
36. Wang XS, Palero V, Soria J, Rhodes MJ. Laser-based planar imaging of nano-particle fluidization: part II—mechanistic analysis of nanoparticle aggregation. *Chem Eng Sci*. 2006;61(24):8040–8049.
37. Wang XS, Rahman F, Rhodes MJ. Nanoparticle fluidization and Geldart's classification. *Chem Eng Sci*. 2007;62(13):3455–3461.
38. Valverde JM, Castellanos A. Fluidization of nanoparticles: a simple equation for estimating the size of agglomerates. *Chem Eng J*. 2008;140(1–3):296–304.
39. Rabinovich E, Kalman H. Pickup, critical and wind threshold velocities of particles. *Powder Technol*. 2007;176(1):9–17.

Manuscript received June 10, 2016, and revision received Sep. 23, 2016.